Journal of Geophysical Research: Atmospheres

RESEARCH ARTICLE
10.1029/2018JD029242

Characteristics of Coastal Low-Level Jets in the Bohai Sea, China, During the Early Warm Season

Fan Zhang[1], Qinghong Zhang[1], Yu Du[2], and Hoiio Kong[1]

[1]Department of Atmospheric and Oceanic Sciences, School of Physics, Peking University, Beijing, China, [2]Center for Monsoon and Environment Research, School of Atmospheric Sciences, and Guangdong Province Key Laboratory for Climate Change and Natural Disaster Studies, Sun Yat-sen University, Guangzhou, China

Key Points:
- CLLJs frequently occur in May when low pressure is located to the north and the Pacific high is located to the southeast of the Bohai Sea
- Inertial oscillation caused by land-sea thermal contrast triggers nocturnal jets in Bohai Sea
- Complicated coastal topography enhances atmospheric baroclinicity and therefore generates afternoon CLLJs in the northern Bohai Sea

Supporting Information:
- Supporting Information S1

Correspondence to:
Q. Zhang,
qzhang@pku.edu.cn

Citation:
Zhang, F., Zhang, Q., Du, Y., & Kong, H. (2018). Characteristics of coastal low-level jets in the Bohai Sea, China, during the early warm season. *Journal of Geophysical Research: Atmospheres*, *123*, 13,763–13,774. https://doi.org/10.1029/2018JD029242

Received 25 JUN 2018
Accepted 1 DEC 2018
Accepted article online 7 DEC 2018
Published online 28 DEC 2018

Abstract We investigate coastal low-level jets (CLLJs) in the early warm season during 2006–2011 over the Bohai Sea using a 9-km horizontal resolution output data from the Weather Research and Forecasting model. CLLJs mainly occur in May when large-scale low is located over land to the north and the Pacific high is located to the southeast of the study area. The occurrence of the CLLJs exhibits an obvious diurnal cycle with two different peaks: one at night, located mainly in the central region, and the other in the afternoon, located in the northern region with mountains at both eastern and western sides. A momentum budget analysis shows that inertial oscillations, triggered by land-sea thermal contrast, results in the formation of nocturnal CLLJs in the Bohai Sea. In addition, sensitivity experiments show that the enhanced atmospheric baroclinicity, caused by unbalanced solar radiation over the western mountain of the northern region, dominates the occurrence of afternoon CLLJs in the northern area of the Bohai Sea. Besides that, the eastern topography plays a main role as barrier and, therefore, traps CLLJs by topography blocking to its western side.

1. Introduction

Coastal low-level jet (CLLJ) is a type of low-level jets (LLJs) that often occurs along the coast (Ranjha et al., 2013). These jets can affect coastal aerosol transportation, low-level clouds, and coastal trapped weather disturbances (Liu et al., 2014); thus, they play an important role in coastal weather and have significant impacts on human activities (Liu et al., 2014). Several studies have focused on the spatial and temporal distribution of CLLJs in various regions. Winant et al. (1988) reported that CLLJs tend to occur in eastern midlatitude oceanic areas where strong cold ocean currents exist. Using 40-km resolution model output data, Rife et al. (2010) elucidated the global distribution of CLLJs in both the cold and warm seasons and found high-frequency CLLJ areas, including the west coast of North America (Burk & Thompson, 1996; Parish, 2000), the Iberian Peninsula (Soares et al., 2017), northwestern Africa (Pu & Cook, 2010, 2012), the southeastern coast of the Arabian Peninsula (Ranjha et al., 2015), the west coast of South America (Garreaud & Munoz, 2005; Q. Jiang et al., 2010; Munoz & Garreaud, 2005), and the coasts of Australia (Ranjha et al., 2013) and southern Africa (Nicholson, 2010). These CLLJs have been widely studied and well documented. Improving on model resolution to 9 km using WRF (Weather Research and Forecasting model), Du et al. (2014) documented the detailed spatial distribution of LLJs over land of China during 2006–2011. Figure 5 in their paper shows three areas of CLLJs along the Chinese coast (the Bohai Sea, Taiwan Strait, and Beibu Gulf), although their study focused mainly on LLJs over the Chinese mainland.

Two main theories have been proposed to explain the occurrence of LLJs. Blackadar (1957) suggested that the supergeostrophic LLJs frequently observed at night resulted from the inertial oscillations in the ageostrophic wind triggered by the sudden decay of eddy viscosity after sunset, while Holton (1967) emphasized the important role of thermal forcing in the diurnal oscillations in the boundary layer wind above sloping terrain where there is unbalanced solar radiation heating. Since the diurnal variation of surface temperature gradient modifies the atmospheric baroclinic, thermal wind mechanism drives geostrophic wind presenting a diurnal cycle: low-level geostrophic wind is stronger than upper-level geostrophic wind during daytime, while the nocturnal condition is reversed (Parish, 2016; Stensrud, 1996). Most recent studies combine these two mechanisms (Du & Rotunno, 2014; X. Jiang et al., 2007; Shapiro et al., 2016).

Compared with nocturnal LLJs, CLLJs differ in various ways in their formation and development mechanisms. Since there is an absence of obvious changes in eddy viscosity within a single day over the sea, inertial oscillations are often triggered by the thermal contrast between the land and ocean (Du et al., 2015; Parish, 2016).

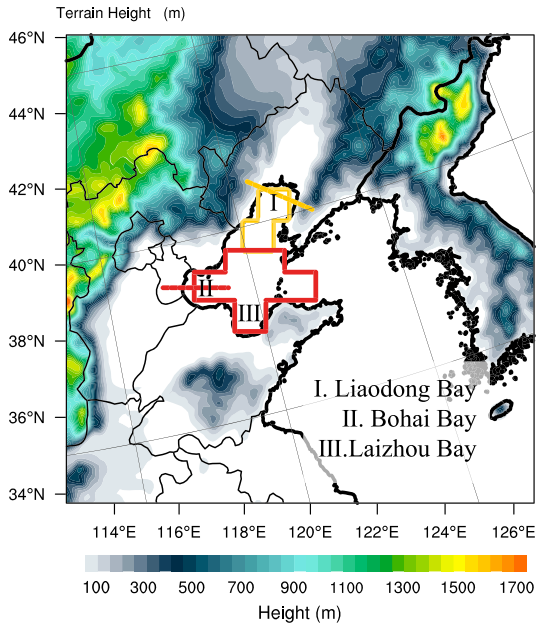

Figure 1. Model terrain height (m, shading) of northeast coastal of China.

CLLJs tend to occur in baroclinic atmospheric conditions, where the surface thermal contrast is sufficiently large (Ranjha et al., 2013). Therefore, many CLLJs are characterized by a midafternoon wind speed maximum affected by enhanced baroclinicity due to the diurnal variation in solar radiation (Winant et al., 1988). Similarly, CLLJs frequently occur over areas of cold currents, where sea surface temperatures are relativity lower than other areas, during the warm season (Ranjha et al., 2013; Soares et al., 2017; Winant et al., 1988). Another key factor in the formation of CLLJs is the coastal terrain (Burk & Thompson, 1996; Cui et al., 1998; Doyle, 1997), since flow can speed up or change direction by interacting with the coastal topography (Jun & Yi-Leng, 1998; Lin et al., 2011; Ridgway & Dunn, 2003). Therefore, detailed studies of CLLJs should consider all the above-mentioned factors. However, compared with LLJs over land, lack of observations over the ocean restricts studies on CLLJ. So far, CLLJs in China have not been well studied in the past. Du et al. (2015) documented the characteristics of CLLJs in the Taiwan Strait using high-resolution model data. They found that the main factor that determined the existence of these CLLJs is large-scale forcing enhanced by land-sea thermal contrast, whereas the topographical effect of the Taiwan and Fujian terrain played a secondary role in the development of the CLLJs near the strait. Based on climate model, Li et al. (2018) depicted the climatology feature of CLLJs in Bohai Sea and Yellow Sea; they showed that CLLJs in these areas have strong interannual, intra-annual, and diurnal cycle variability but weak decadal variability. Nevertheless, the detailed mechanisms involved in CLLJs in Bohai Sea of China are still unclear.

The Bohai Sea, which contains six of China's 10 main coastal ports, is one of the busiest seaways in the world. The near-surface high-speed wind maximum caused by CLLJs may lead to uncertainty to navigation. In terms of topography, there are three major bays inside the Bohai Sea (Figure 1): Laizhou Bay to the south, Liaodong Bay to the north, and Bohai Bay to the west. Furthermore, Liaodong Bay is enclosed by mountains on both eastern and western sides. Thus, the coastline of the Bohai Sea has a complicated form. Previous studies, which explored mechanisms behind the formation and variation of CLLJs, mainly focused on relatively straight coastal area, such as the south and east coast of China (Du et al., 2015; Lin et al., 2011) and the west coast of Chile (Q. Jiang et al., 2010). Their results cannot provide an all-sided explanation that is suitable for CLLJs occurring in such a complex coastal topography system in Bohai Sea. Hence, further studies in Bohai Sea are important for both local ports' navigation safety and understanding of the interactions between complicated coastal topography and CLLJs.

In this study, we use the output data from WRF for six early warm seasons (May–July 2006–2011) to explore the distribution, formation mechanisms, and diurnal variations of the CLLJs in the Bohai Sea. The data and methods are described in section 2, which is followed by an analysis of the temporal and spatial distributions of the CLLJs over the Bohai Sea in section 3. Section 4 describes the formation and development mechanisms of the CLLJs. Finally, the results of our study are summarized in section 5.

2. Data and Methodology

2.1. Definition of CLLJs and Data Specification

We define CLLJs using the criteria in Du et al. (2014), as follows: (1) the maximum wind speed is greater than 10 m/s and (2) the wind speed must decrease by at least 3 m/s from the height of maximum wind speed to the height of minimum wind speed above (occurring below the eighth model layer, approximately below the 1-km level). We also define the position of a CLLJ in vertical direction as the height where it has the maximum horizontal wind velocity and identify the wind profile of each model grid as an event. To distinguish CLLJ days from other days, we chose 300 model grids, covering a core zone (38°12′–39°48′N, 119–121°E) of the Bohai Sea, which yield 7,200 events (300 grids multiplied by 24 hr) per day. Based on this, for any specified area, we define CLLJ days as those on which more than 50% of the events (i.e., 3,600 events) satisfy the CLLJ criteria and non-CLLJ days as the remaining days.

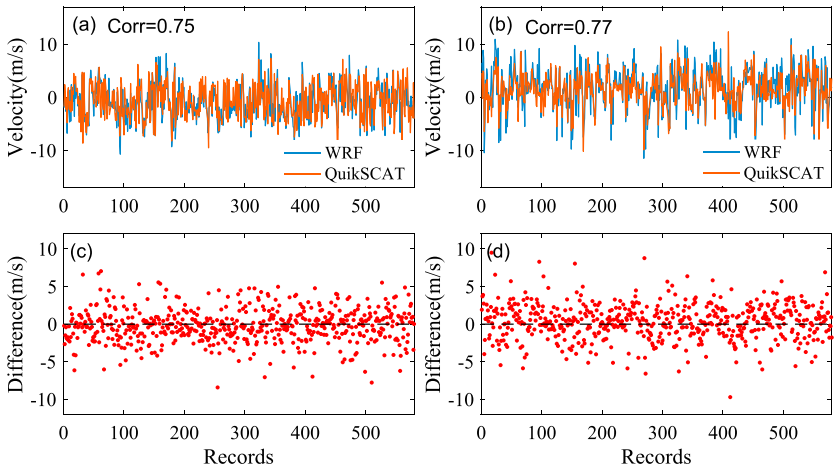

Figure 2. Comparison between model wind velocity (m/s) and Quick Scatterometer (QuikSCAT) observation velocity (m/s) at 10 m (top row); difference of each record (bottom row). (a and c) *U* direction; (b and d) *V* direction from May to July during 2006–2009.

The hourly model data used in this study are outputs from the WRF model, with a horizontal grid spacing of 9 km and 40 vertical levels. Within the lowest 1 km from surface, there are eight levels in this model so that it can easily capture the vertical characteristics of the lower atmosphere. The domain encompasses the entire region of the Bohai Sea from May to July during 2006–2011. To verify the quality of the model data in the Bohai Sea, a 0.25° × 0.25° Earth grid data set observed from the Quick Scatterometer (QuikSCAT, a satellite-based SeaWinds instrument) including wind speed and direction at the height of 10 m above ocean surface is used for comparison. Ricciardulli and Wentz (2015) documented high accuracy and low uncertainty in wind speed up to 30 m/s, for rain-free measurements. Although at low winds in heavy rain the wind bias might increase, the rain flag in QuikSCAT shows that rain rarely (less than 15%) occurs in Bohai Sea during our simulation period. Two records are retrievable from QuikSCAT for each day: one from ascending orbit segments (0600 LST) and the other from descending orbit segments (1800 LST). Besides that, QuikSCAT was launched in June 1999 and operated until November 2009. Following this, we chose data from 2006 to 2009 to verify the reliability of the model data.

2.2. Data Validation

The average surface wind speeds detected by QuikSCAT in the core zone of the Bohai Sea are calculated, and corresponding model data outputs are extracted. When missing data are excluded, there is a total of 592 wind speed records in the U and V directions.

Figures 2a and 2b compare all the records of model output and satellite observation in both directions. The Pearson correlation coefficients in the U and V directions are 0.75 and 0.77, respectively ($p < 0.05$). In addition, we analyze the residual term to determine whether the differences result from random error. Figures 2c and 2d show that differences (WRF model output minus QuikSCAT observation) between the two data sets are spread randomly around 0. The standard deviation of the differences satisfies the null hypothesis of a one-sample *K-S* test, indicating that the standard deviation of the differences meets the requirements of standard normal distribution. These statistical analyses show that the model produces a satisfactory simulation of actual conditions.

3. Characteristics of CLLJs

3.1. Temporal Distribution

Figure 3 shows the monthly mean horizontal distribution of the frequency of CLLJs during 2006–2011. CLLJs occur in the Bohai Sea mainly in May when a low-pressure system is located to the north and the Pacific high is located to the southeast (Figure 4a). Under this condition, near-surface coastal winds parallel to the seashore (Figure 3a) are conducive to the development of CLLJs (Pomeroy & Parish, 2001; Ranjha et al., 2013). In June and July, accompanied by the northward movement of the Pacific high (Figures 4b and 4c),

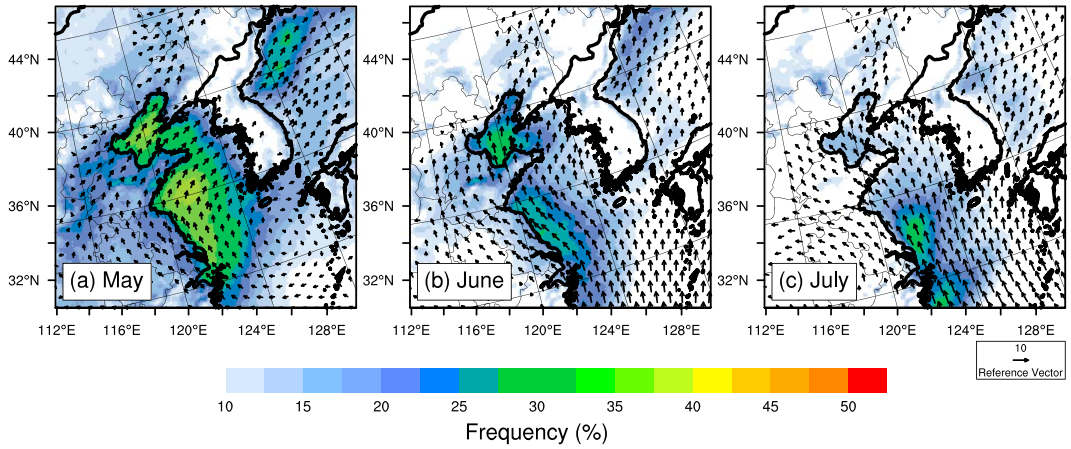

Figure 3. Horizontal distributions of frequency of coastal low-level jets (%, shading); wind in 975 hPa (vectors) in (a) May, (b) June, and (c) July, averaged from 2006 to 2011. Vectors under mountains are not shown.

meridian circulation dominates the Bohai Sea. Low-level winds rotate anticlockwise and ultimately have a strong component that blows toward the coastline (Figures 3b and 3c). Since CLLJ tend to occur when background wind blows along coastal line, wind direction in June and July is a negative factor for CLLJ development. Hence, the frequency of CLLJs continually decreases.

3.2. Spatial Distribution

Although Figure 3a shows a high-frequency CLLJ region over the Bohai Sea in May, the monthly average wind speed over the sea is significantly lower than the CLLJ velocity threshold (10 m/s). The reason for this phenomenon is the counteraction between different wind directions. The large-scale circulation in May drives background winds in the sea in a southwesterly direction (Figure 3a). However, fast-moving baroclinic cyclones, which are very common at synoptic scale in midlatitudes, cause frequent variations in the wind direction in May. Figure 5 shows the distribution of wind direction in May. Roughly 70% of the wind direction in the Bohai Sea is southwesterly (including southerly and westerly). On CLLJ days, southwesterly winds still dominate, and their proportion increases to 80%. By contrast, the proportion of wind from other directions is far smaller than that from the southwest. This consequence is similar to the 35-year regional climate model analysis in Bohai Sea (Li et al., 2018). It should be noted that in our analysis, days with background winds from nonsouthwesterly directions are filtered out to avoid confusion among different wind directions.

Besides that, CLLJs occur over different areas in the Bohai Sea during a single day. Figure 6 shows the horizontal distributions of CLLJ frequency at 3-hr intervals from 1400 to 0500 LST. CLLJs occur in the northern area of the Bohai Sea in the afternoon (afternoon CLLJ events, from 1400 to 1900 LST) and in the central area at night (nocturnal CLLJ events, from 2200 to 0300 LST). Therefore, we divide the Bohai Sea into two regions: an afternoon high-frequency region (northern region, indicated by yellow boxes in Figure 1) and a nocturnal high-frequency region (central region, indicated by red boxes in Figure 1). In vertical direction, both jets of

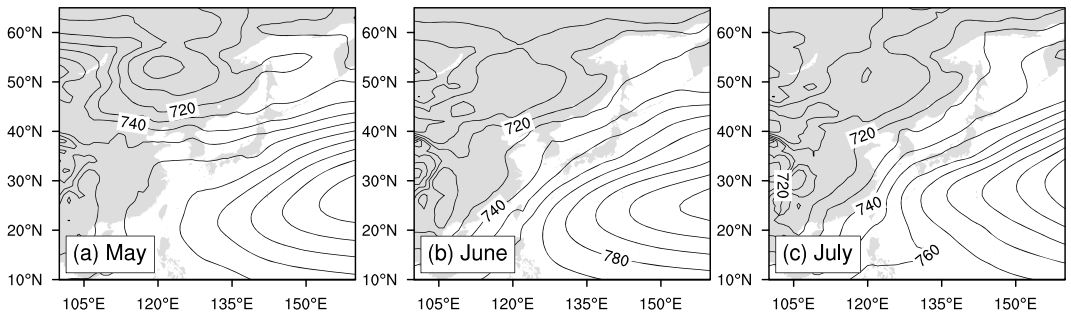

Figure 4. Large-scale circulation at 925 hPa averaged over 2006–2011 in (a) May, (b) June, and (c) July. Contour lines represent geopotential height (m).

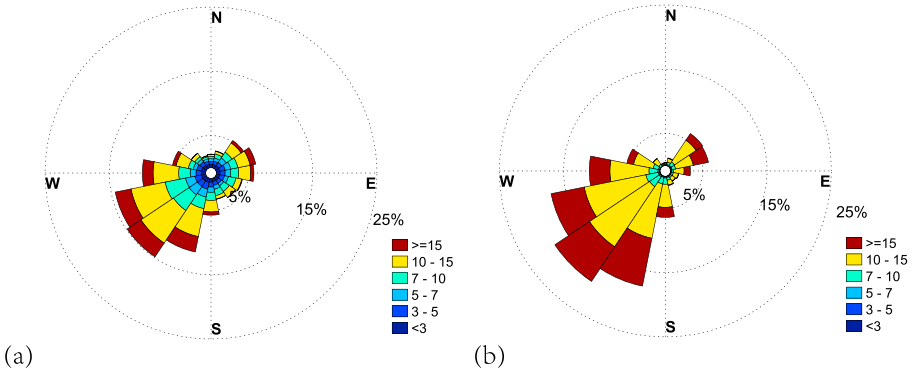

Figure 5. Wind direction and velocity (m/s, shading) distributions (%) of (a) all wind events and (b) coastal low-level jet events in Bohai Sea in May from 2006 to 2011.

these two regions are located at 975 hPa (Figure 7). So in the following sections, we focus on this height to do further research.

4. Formation Mechanisms

4.1. Large-Scale Effects

We use the 6-hourly Final (FNL) operational global analysis data, with 1° × 1° grid spacing and 28 levels from National Centers for Environmental Prediction to examine the effect of large-scale circulation in this section. By comparing the distinction of large-scale background circulation between CLLJ and non-CLLJ days (Figure 8), pressure gradient at 925 hPa over the Bohai Sea region on CLLJ days is significantly stronger than that on the non-CLLJ days. Therefore, geostrophic wind in CLLJ days is stronger than that in non-CLLJ days. Since geostrophic wind is a main component of jet stream, CLLJs tend to occur under conditions with intensive large-scale geostrophic winds. By analyzing all the days in May from 2006 to 2011, we find that the intensity of background pressure gradient in 2007 and 2010 is obviously lower than other years (Figure S1 in the supporting information). Since a key criterion of CLLJ is a minimum threshold wind speed of 10 m/s, in the following section we choose data in 2006, 2008, 2009, and 2011 to analyze dynamic mechanism.

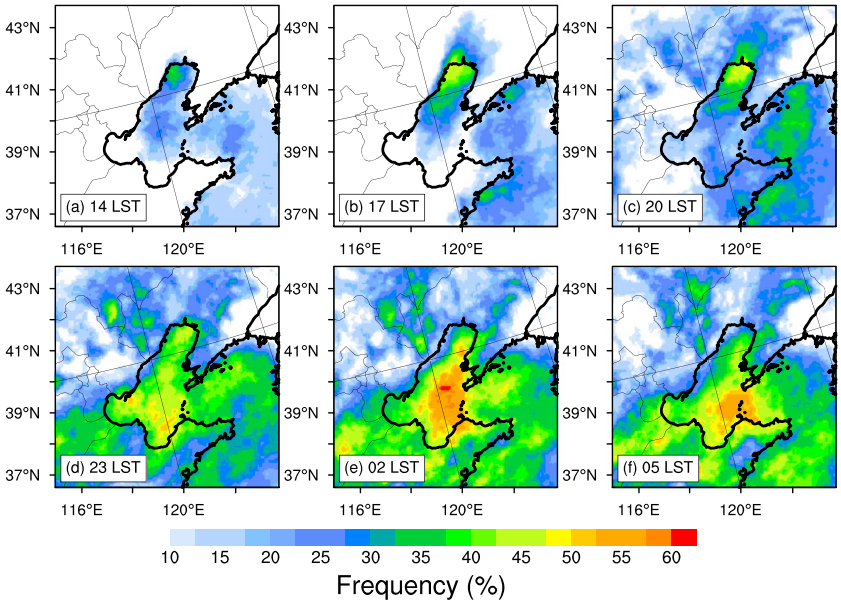

Figure 6. Horizontal distribution of frequency (%, shading), every 3 hr from 1400 to 0500 LST, of low-level jets in northeast coastal area of China: (a) 14 LST; (b) 17 LST; (c) 20 LST; (d) 23 LST; (e) 02 LST; and (f) 05 LST.

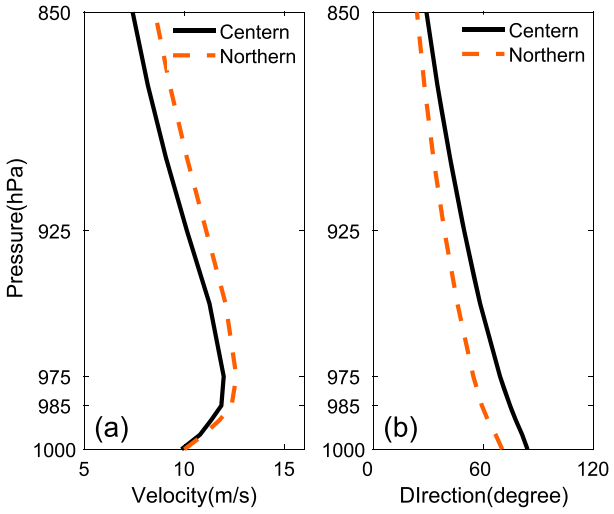

Figure 7. Vertical profile of (a) wind velocity (m/s) and (b) wind direction (degrees) averaged over central region (black solid line) and northern region (red dash line).

4.2. Diurnal Variation

Under similar large-scale conditions, variations in winds show different patterns between the central and northern regions. To investigate the roles of the different wind components in the development of CLLJs, diurnal variations in both actual winds and geostrophic winds are examined (Figure 9). It is worth noting that the differences between actual wind and geostrophic wind represent ageostrophic wind. In the central region, the geostrophic wind fluctuates only slightly from 6.0 to 8.5 m/s, whereas there is significant diurnal variation in geostrophic wind in the northern region, which is from 6.6 to 12.3 m/s. Ageostrophic winds also play different roles in the formation of CLLJs (deceleration for afternoon jet events in the northern region and acceleration for nocturnal jet events in both regions). To explain the effects of different forces in the diurnal variation in CLLJs, we analyze the momentum budgets in the two regions.

4.3. Central Region

The horizontal momentum equation (equation (1)) can depict horizontal motion of air parcel. Tendency of motion which is represented by local derivative of the *y* component wind (Ten) equals the sum of horizontal advection (Adv), vertical advection (Ver), Coriolis force acting on the ageostrophic wind in the *x* direction (Cor), and friction (Res) terms.

$$\underbrace{\frac{\partial v}{\partial t}}_{\text{Ten}} = \underbrace{\left(-u\frac{\partial v}{\partial x} - v\frac{\partial v}{\partial y}\right)}_{\text{Adv}} \underbrace{- w\frac{\partial u}{\partial z}}_{\text{Ver}} \underbrace{- f\left(u - u_g\right)}_{\text{Cor}} + \underbrace{F_y}_{\text{Res}} \tag{1}$$

It is worth noting that the coordinate transformation (Du & Rotunno, 2014; Zhang et al., 2003) can be used to visually represent the effects of each term in the momentum budget. The coordinate orientation for *y* corresponds to the maximum CLLJ direction. The variables in the other direction are projected onto the *y* coordinate.

We examine the momentum budget of horizontal wind at the 975-hPa level over the central region in May (Figure 10a). Compared with other terms, the diurnal variation of the Adv, Ver, and Res terms are

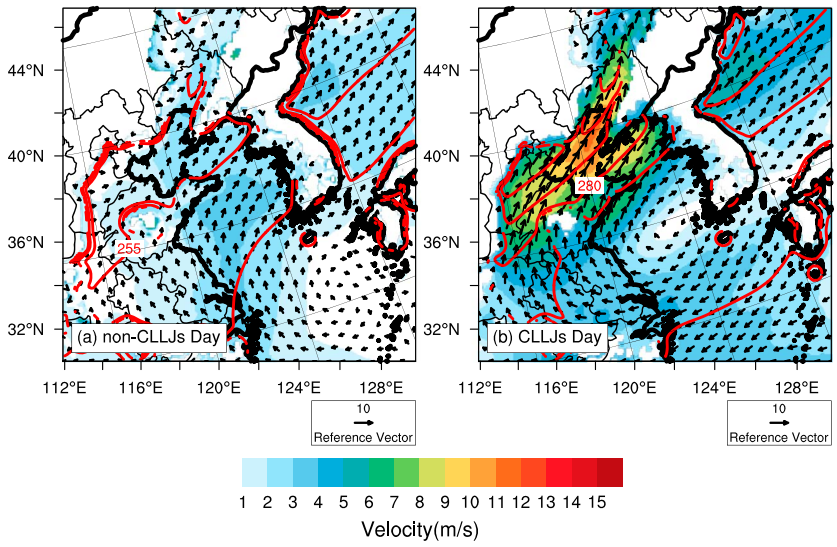

Figure 8. Geopotential height (m, contour lines), horizontal wind velocity (m/s, shading), and direction (vector) at 925 hPa for (a) non-CLLJs day and (b) CLLJs day. Contour lines and shading under mountains are not shown. CLLJ = coastal low-level jet.

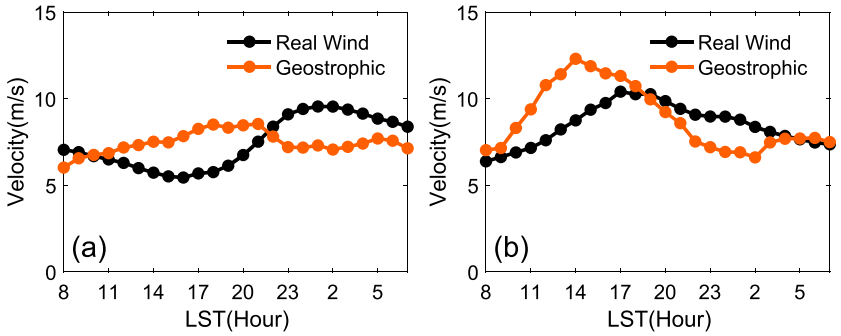

Figure 9. Diurnal variations of wind; black lines denote the actual wind, and red lines denote geostrophic wind averaged (at 975 hPa) over the (a) central region and (b) northern region.

relatively small; thus, the effects from these three terms in this region could be ignored. By contrast, Cor term varies obviously and dominates the variation of the local velocity during the whole day. That is because the total wind in the central region is significantly accelerated by ageostrophic component (Figure 9a) at night. So far, the primary question that needs to be answered is the source of this ageostrophic wind. The theory that land-sea thermal contrast can result in a thermal circulation along the coast has been well documented (Atkins et al., 1995; Haurwitz, 1947; Rotunno, 1983). In the central region, since the land to the west is heated by the solar radiation, the temperature contrast between land and sea is enhanced in the afternoon (Figures 11f–11h). Hence, a thermal circulation (Figure 12a, downdraft [updraft] exists over sea [land] and low-level wind blows toward the land) is triggered around noon and then strengthens until sunset due to continual heating by solar radiation over the land. Because of inertial oscillation, the ageostrophic wind in the central region rotates clockwise (blue line in Figure 11i). At midnight, the southwesterly ageostrophic wind enhances the background wind in Bohai Sea (Figure 9a). Thus, this Blackadar's (1957) inertial oscillation mechanism (triggered by radiation diurnal variation) explains the occurrence of nocturnal CLLJs in the central region. This mechanism is similar to the dynamics of CLLJs in Taiwan Strait (Du et al., 2015).

4.4. Northern Region

The phase of the wind components (Figure 9) in the northern region differs significantly from that in the central region; thus, CLLJs in the northern region cannot be explained simply by land-sea thermal contrast and inertial oscillations. The geostrophic wind speed in the northern region (Figure 9b) increases from 0800 LST and reaches its peak strength (12.6 m/s) at 1400 LST. Although ageostrophic wind plays a diminished role during afternoon CLLJ events, actual wind still exceeds the threshold (10 m/s^{-1}) for formation of CLLJ due to the geostrophic wind being sufficiently strong.

Several studies have documented how enhanced land-sea thermal contrast can result in more pronounced baroclinicity (Burk & Thompson, 1996; Q. Jiang et al., 2010; Kottmeier et al., 2000). Thus, the geostrophic wind can be strengthened over coastal areas due to increased solar radiation in the afternoon. However, this still

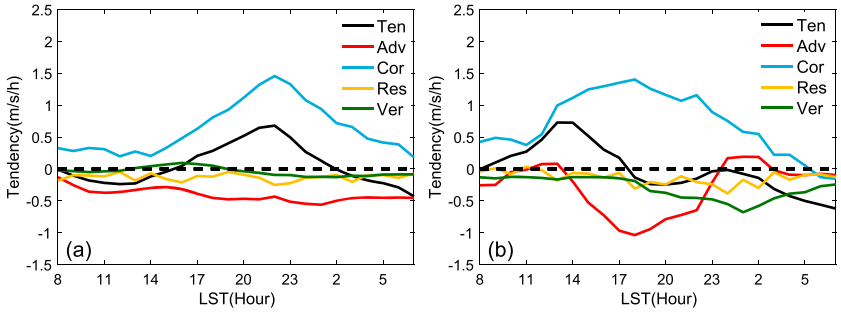

Figure 10. Diurnal variations of individual terms ($m{\cdot}s^{-1}{\cdot}hr^{-1}$) in the horizontal momentum equation at the 975-hPa level (a) averaged over the central region (red box in Figure 1a) and (b) averaged over the northern region (yellow box in Figure 1a).

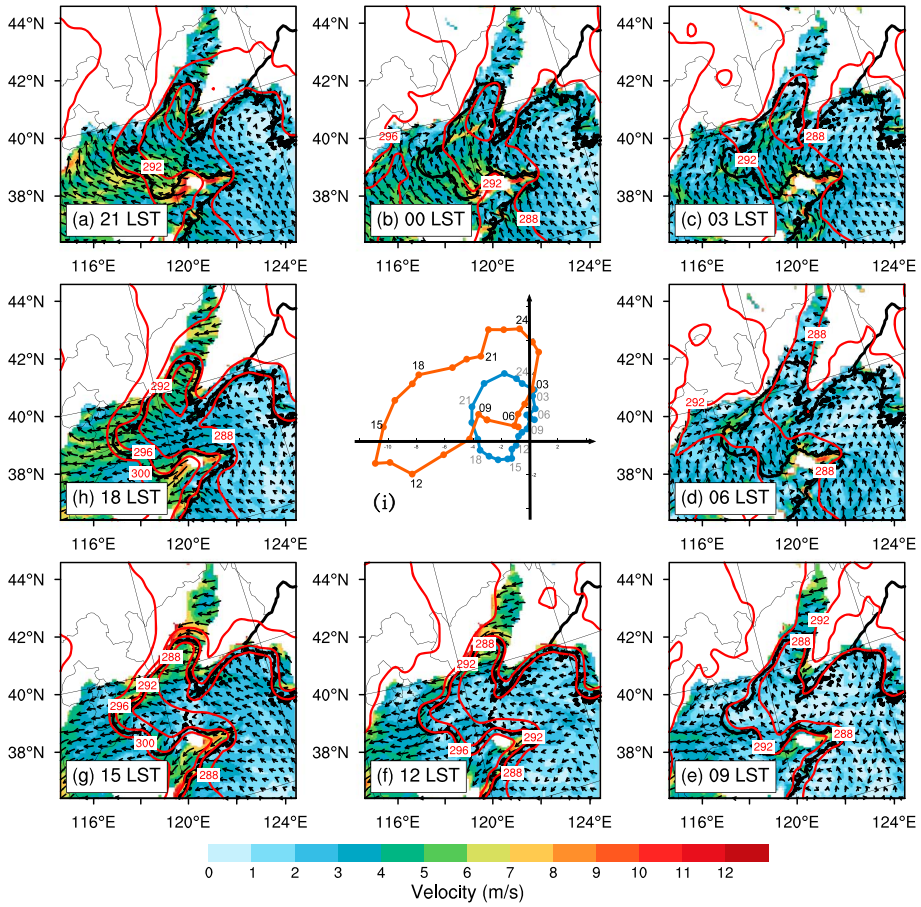

Figure 11. (a–h) Spatial distribution of the surface potential temperature (K, contour line) and ageostrophic wind vectors of 975 hPa at 0000, 0300, 0600, 0900, 1200, 1500, 1800, and 2100 LST averaged over May. (i) The blue (red) line represents clockwise rotation of 975-hPa ageostrophic wind averaged over central (northern) region. Contour lines and shading under mountains are not shown.

does not explain why the diurnal variation in the geostrophic wind in the northern region is much stronger than that in the central region. Therefore, we further investigate the effects of topography derived from the surrounding terrain.

4.4.1. Topographical Effects

Around Bohai Sea (Figure 1), a large-scale sloping topography is located to the west of north Bohai region, while a windward topography is found to the east. According to the following analysis in this section, both these two mountains' effects on CLLJ generation are unveiled.

From the view of solar radiation, a sloping topography can change the horizontal distribution of surface solar heating rate (Paegle & Rasch, 1973; Stensrud, 1996). Compared with the flat land around the central region (Figure 1), the west side of the northern region is sloping topography where surface gains more solar radiation during afternoon (Figures 12a and 12c), and therefore, isothermal lines tilt obviously toward the west land of the northern region; coastal surface thermal gradient is also greater than the central region (Figures 11e–11h). As a result, atmospheric baroclinicity enhances remarkably. In addition, corresponding with thermal wind mechanism, geostrophic wind decreases from surface to upper level (Figure 12c) during afternoon. Since the vertical wind shear is a criterion of defining CLLJ, this vertical profile of geostrophic wind is also beneficial to generate jet events.

From the view of fluid dynamic, a windward topography could have a role as a barrier. The condition that determines whether an air parcel cloud rise up and over a mountain is determined by the Froude number (equation (2)). In this case, the kinetic energy is represented by the wind speed (*U*), whereas the potential

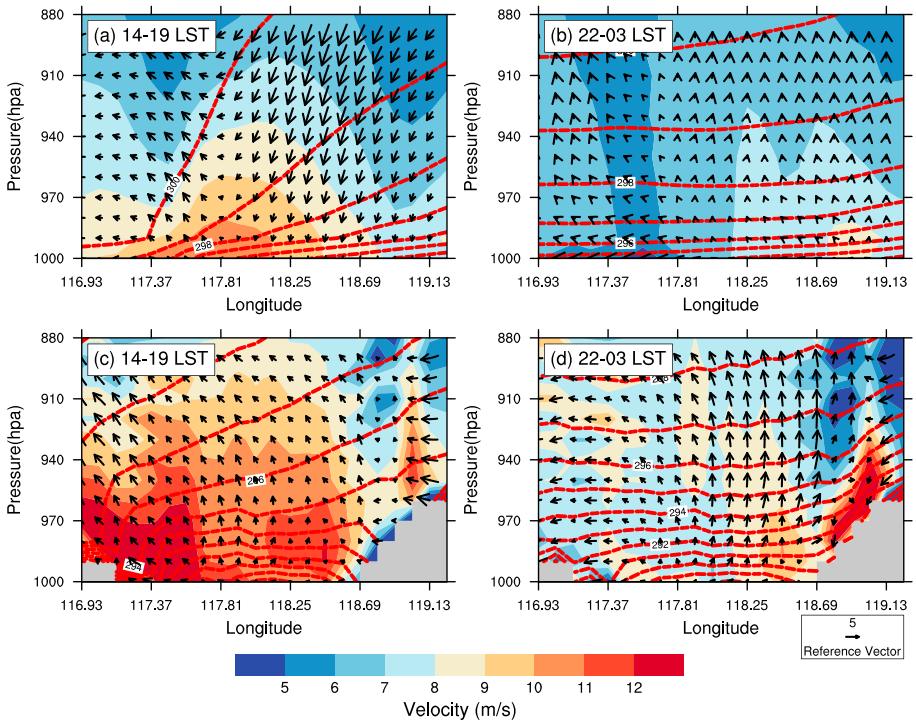

Figure 12. Geostrophic wind flow into this section (m/s, shading), vertical circulation in this cross section (horizontal wind and vertical wind multiply by 250, m/s, vectors), and potential temperature (K, red dashed line) of cross section: (a and b) represented by the red line in Figure 1; (c and d) represented by the yellow line in Figure 1.

energy is represented by the Brunt-Väisälä frequency (N) multiplied by the height of the mountain (H_m). If the Froude number is greater than 1, then flow cloud passes over the mountain; if the Froude number is less than 1, then flow will be blocked by the mountain.

$$Fr = \frac{U}{N \cdot H_m} \tag{2}$$

For air parcel at 990-hPa level near the eastern mountain of north Bohai region (where N is 0.03 and H_m is 328 m), if we assume Fraud number greater than 1, the critical velocity which is perpendicular to the mountain should exceed 9.8 m/s. However, the actual velocity (1.78 m/s) is significantly less than this threshold. After calculating the Fraud number of all the level below the mountain top in the northern region, 970-hPa level is the critical layer where Fraud number is 1. Therefore, this simple physical mechanism suggests that air parcel in the northern region below 970 hPa is essentially blocked by the eastern mountain. Thus, a shallow high-pressure area generates next to the mountain, and the low-level horizontal pressure gradient force is not balanced by Coriolis and friction forces (Carrera et al., 2009; Gaberšek & Durran, 2006). Hence, the geostrophic wind starts to accelerate under geostrophic adjustment. Through this process, wind within the channel is deflected and eventually aligning with the mountain. As a consequence, a barrier jet generates on the left base side of the eastern mountain. By contrast, flow without the channel is similar to synoptic-scale geostrophic wind. This barrier effect explains why it seems that CLLJs in the northern region are trapped in the channel between two side topographies (Figures 3a and 6).

4.4.2. Sensitivity Experiments

Based on the above theory analyses, we have already got a general knowledge about CLLJ formation in Bohai Sea. In this section, we further verify our results and quantitatively compare the importance of both side topographies on generating northern region CLLJs by sensitivity experiments. Two model sensitivity experiments are shown below: (1) NoFlux experiment where surface heat and moisture fluxes are turned off and (2) LowEM where the eastern mountain height is reduced to 10% of the actual height. Compared with the run control (Figures 13a and 13b), the afternoon peak and the strong diurnal variation of geostrophic wind disappears when we turned off the surface flux (Figures 13c and 13d). By contrast, since the eastern

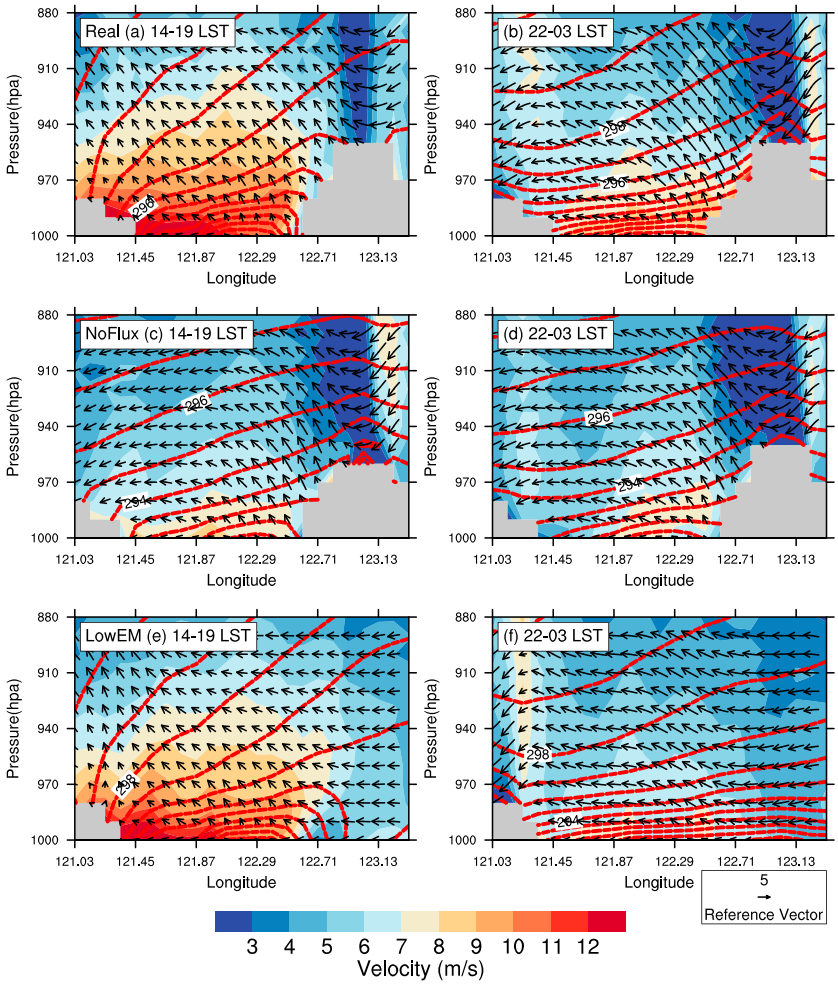

Figure 13. Wind velocity (m/s, shading), wind in this cross section (horizontal wind and vertical wind multiply by 250, m/s, vectors), and potential temperature (red dash line, K) of cross section represented by yellow line in Figure 1. (a and b) Real experiment, (c and d) NoFlux experiment, and (e and f) LowEM experiment.

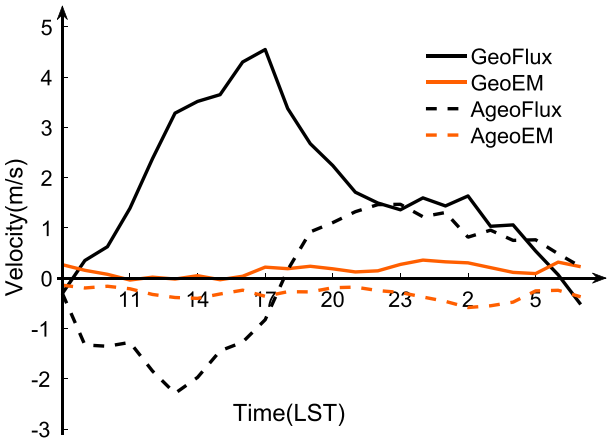

Figure 14. Diurnal variation of surface flux and the eastern mountain's contribution on geostrophic wind (solid line, m/s) and ageostrophic wind (dash line, m/s) averaged over northern region.

mountain continued interacting with windward side flow, the barrier enhancement still exists (Figures 13c and 13d). In LowEM sensitivity experiment, when the eastern mountain is reduced to 10% of the actual height, the afternoon geostrophic wind does not have an obvious change in the northern region (Figure 13e), while the topography enhancement is weakened (Figure 13f).

The quantified calculation results (averaged over the whole northern region) and the difference of both geostrophic and ageostrophic wind between run control and each sensitivity experiment in jet direction are shown in Figure 14. For geostrophic wind, the thermal effect dominated by the western mountain contributes an obvious diurnal variation of velocity with the maximum 4.5-m/s enhancement at 1700 LST and the maximum −0.5-m/s deceleration at 0600 LST. In comparison, the eastern mountain's contribution on geostrophic wind is always positive but limited, which just fluctuates around 0.3 m/s. For ageostrophic wind, the contribution of the two sides' topography is totally different. Under the effect of the western topography driving thermal effect, ageostrophic wind will

present a clockwise rotation (Figure S2). Hence, in jet direction, the western topography triggering ageostrophic wind (Figure 14) has a maximum deceleration effect (−2.3 m/s) at 1300 LST and a maximum acceleration effect (1.8 m/s) at 2300 LST. However, since the ageostrophic wind generated by the eastern topography always blows backward to the barrier, it does not have an obvious diurnal change on direction (Figure S2). So it only has a slight deceleration effect on actual wind from day to night. After being averaged over the northern region, topography blocking driving geostrophic acceleration is generally counteracted by the ageostrophic deceleration.

From another perspective, we verify the contribution of both sides of the mountain on the occurrence of CLLJs (Figure S3). The western topography driving radiation effect contributes 41.6% afternoon CLLJ events, while the eastern topography blocking does not have an obvious influence on frequency in the northern region. Hence, the afternoon CLLJs are dominated by the western topography.

5. Conclusion

We use hourly WRF model output with 9-km horizontal resolution and 40 levels in vertical direction to examine the mechanisms of the formation and development of CLLJs in the Bohai Sea in the early warm season (May–July) during 2006–2011. By analyzing this model data and two more sensitivity experiments, we elucidate the main characteristics of the mechanisms that drive the diurnal variations in CLLJs in the Bohai Sea. The main findings are summarized below.

1. CLLJs occur in the Bohai Sea mainly in May when there is a strong large-scale horizontal pressure gradient that is driven by subtropical high over ocean and low system over land. Under this background, CLLJs tend to occur when background winds are intensive and southeasterly.
2. There are two regions (northern and central) where the peak strengths, diurnal variations, and driving mechanisms of CLLJs differ between each other.

In the central region, enhanced land-sea thermal contrast that occurs in the afternoon drives a stronger low-level ageostrophic wind, which blows in onshore direction. After sunset, this thermal contrast gradually disappears. Without a persistent thermal forcing, ageostrophic wind is rotated by Coriolis force. CLLJs generate when ageostrophic wind has a strong component on geostrophic wind direction (from 2100 to 1000 LST). Thus, inertial oscillation triggered by land-sea thermal contrast plays the main role in triggering CLLJs and the diurnal wind variations.

In the northern region, CLLJs generate at 1400 LST and disappear at 0400 LST. The sloping land to the west of the northern region enhances the solar radiation gradient of the surface; then, atmospheric baroclinicity is intensified more remarkably than the central region. The intensive near-surface geostrophic wind mainly contributes to CLLJ in the afternoon, while the eastern topography (blocking and channeling) trap these jets to the west of itself.

This is the first time that the mechanism of CLLJs in Bohai Sea is explored under such a complex coastal line and topography condition. Our results may shed light on understanding the formation mechanism of CLLJs in other regions of the world. However, due to lack of sound observations across the Bohai Sea, our results need verification in future observations and experiments in this area.

Acknowledgments
This study is supported by the Chinese National Science Foundation under grants 41875052 and 41875055. We use QuikSCAT data and NCEP FNL analysis in our study. QuikScat (or SeaWinds) data are produced by Remote Sensing Systems and sponsored by the NASA Ocean Vector Winds Science Team. Data are available at www.remss.com. National Centers for Environmental Prediction/National Weather Service/NOAA/U.S. Department of Commerce (2000), NCEP FNL Operational Model Global Tropospheric Analyses, continuing from July 1999, https://doi.org/10.5065/D6M043C6. Research Data Archive at the National Center for Atmospheric Research, Computational and Information Systems Laboratory, Boulder, Colo. (Updated daily). Accessed 24 September 2018.

References

Atkins, N. T., Wakimoto, R. M., & Weckwerth, T. M. (1995). Observations of the sea-breeze front during CaPE. Part II: Dual-Doppler and aircraft analysis. *Monthly Weather Review*, *123*(4), 944–969. https://doi.org/10.1175/1520-0493(1995)123<0944:OOTSBF>2.0.CO;2

Blackadar, A. K. (1957). Boundary layer wind maxima and their significance for the growth of nocturnal inversions. *Bulletin of the American Meteorological Society*, *38*(5) 283–290.

Burk, S. D., & Thompson, W. T. (1996). The summertime low-level jet and marine boundary layer structure along the California coast. *Monthly Weather Review*, *124*(4), 668–686. https://doi.org/10.1175/1520-0493(1996)124<0668:TSLLJA>2.0.CO;2

Carrera, M. L., Gyakum, J. R., & Lin, C. A. (2009). Observational study of wind channeling within the St. Lawrence River Valley. *Journal of Applied Meteorology and Climatology*, *48*(11), 2341–2361. https://doi.org/10.1175/2009jamc2061.1

Cui, Z. Q., Tjernstrom, M., & Grisogono, B. (1998). Idealized simulations of atmospheric coastal flow along the central coast of California. *Journal of Applied Meteorology*, *37*(10), 1332–1363. https://doi.org/10.1175/1520-0450(1998)037<1332:ISOACF>2.0.CO;2

Doyle, J. D. (1997). The influence of mesoscale orography on a coastal jet and rainband. *Monthly Weather Review*, *125*(7), 1465–1488. https://doi.org/10.1175/1520-0493(1997)125<1465:TIOMOO>2.0.CO;2

Du, Y., Chen, Y.-L., & Zhang, Q. (2015). Numerical simulations of the boundary layer jet off the southeastern coast of China. *Monthly Weather Review*, *143*(4), 1212–1231. https://doi.org/10.1175/mwr-d-14-00348.1

Du, Y., & Rotunno, R. (2014). A simple analytical model of the nocturnal low-level jet over the Great Plains of the United States. *Journal of the Atmospheric Sciences*, *71*(10), 3674–3683. https://doi.org/10.1175/JAS-D-14-0060.1

Du, Y., Zhang, Q., Chen, Y., Zhao, Y., & Wang, X. (2014). Numerical simulations of spatial distributions and diurnal variations of low-level jets in China during early summer. *Journal of Climate*, *27*(15), 5747–5767. https://doi.org/10.1175/jcli-d-13-00571.1

Gaberšek, S., & Durran, D. R. (2006). Gap flows through idealized topography. Part II: Effects of rotation and surface friction. *Journal of the Atmospheric Sciences*, *63*(11), 2720–2739. https://doi.org/10.1175/JAS3786.1

Garreaud, R. D., & Munoz, R. C. (2005). The low-level jet off the west coast of subtropical South America: Structure and variability. *Monthly Weather Review*, *133*(8), 2246–2261. https://doi.org/10.1175/mwr2972.1

Haurwitz, B. (1947). Comments on the sea-BREEZE circulation. *Journal of Meteorology*, *4*(1), 1–8. https://doi.org/10.1175/1520-0469(1947)004<0001:COTSBC>2.0.CO;2

Holton, J. R. (1967). The diurnal boundary layer wind oscillation above sloping terrain. *Tellus*, *19*(2), 200–205. https://doi.org/10.3402/tellusa.v19i2.9766

Jiang, Q., Wang, S., & O'Neill, L. (2010). Some insights into the characteristics and dynamics of the Chilean low-level coastal jet. *Monthly Weather Review*, *138*(8), 3185–3206. https://doi.org/10.1175/2010MWR3368.1

Jiang, X., Lau, N.-C., Held, I. M., & Ploshay, J. J. (2007). Mechanisms of the Great Plains low-level jet as simulated in an AGCM. *Journal of the Atmospheric Sciences*, *64*(2), 532–547. https://doi.org/10.1175/jas3847.1

Jun, L., & Yi-Leng, C. (1998). Barrier jets during TAMEX. *Monthly Weather Review*, *126*(4), 959–971. https://doi.org/10.1175/1520-0493(1998)126<0959:BJDT>2.0.CO;2

Kottmeier, C., Palacio-Sese, P., Kalthoff, N., Corsmeier, U., & Fiedler, F. (2000). Sea breezes and coastal jets in southeastern Spain. *International Journal of Climatology*, *20*(14), 1791–1808. https://doi.org/10.1002/1097-0088(20001130)20:14<1791::AID-JOC574>3.0.CO;2-I

Li, D., von Storch, H., Yin, B., Xu, Z., Qi, J., Wei, W., & Guo, D. (2018). Low-level jets over the Bohai Sea and Yellow Sea: Climatology, variability, and the relationship with regional atmospheric circulations. *Journal of Geophysical Research: Atmospheres*, *123*, 5240–5260. https://doi.org/10.1029/2017JD027949

Lin, P. L., Chen, Y. L., Chen, C. S., Liu, C. L., & Chen, C. Y. (2011). Numerical experiments investigating the orographic effects on a heavy rainfall event over the northwestern coast of Taiwan during TAMEX IOP 13. *Meteorology and Atmospheric Physics*, *114*(1-2), 35–50. https://doi.org/10.1007/s00703-011-0155-7

Liu, H., He, M., Wang, B., & Zhang, Q. (2014). Advances in low-level jet research and future prospects. *Joural of Meteorogical Research*, *1*(40905049), 57–75. https://doi.org/10.1007/s13351-014-3166-8.1

Munoz, R. C., & Garreaud, R. D. (2005). Dynamics of the low-level jet off the west coast of subtropical South America. *Monthly Weather Review*, *133*(12), 3661–3677. https://doi.org/10.1175/mwr3074.1

Nicholson, S. E. (2010). A low-level jet along the Benguela coast, an integral part of the Benguela current ecosystem. *Climatic Change*, *99*(3–4), 613–624. https://doi.org/10.1007/s10584-009-9678-z

Paegle, J., & Rasch, G. E. (1973). Three-dimensional characteristics of diurnally varying boundary-layer flows. *Monthly Weather Review*, *101*(10), 746–756. https://doi.org/10.1175/1520-0493(1973)101<0746:TCODVB>2.3.CO;2

Parish, T. R. (2000). Forcing of the summertime low-level jet along the California coast. *Journal of Applied Meteorology*, *39*(12), 2421–2433. https://doi.org/10.1175/1520-0450(2000)039<2421:FOTSLL>2.0.CO;2

Parish, T. R. (2016). A comparative study of the 3 June 2015 Great Plains low-level jet. *Monthly Weather Review*, *144*(8), 2963–2979. https://doi.org/10.1175/MWR-D-16-0071.1

Pomeroy, K. R., & Parish, T. R. (2001). A case study of the interaction of the summertime coastal jet with the California topography. *Monthly Weather Review*, *129*(3), 530–539. https://doi.org/10.1175/1520-0493(2001)129<0530:ACSOTI>2.0.CO;2

Pu, B., & Cook, K. H. (2010). Dynamics of the west African westerly jet. *Journal of Climate*, *23*(23), 6263–6276. https://doi.org/10.1175/2010jcli3648.1

Pu, B., & Cook, K. H. (2012). Role of the west African westerly jet in Sahel rainfall variations. *Journal of Climate*, *25*(8), 2880–2896. https://doi.org/10.1175/jcli-d-11-00394.1

Ranjha, R., Svensson, G., Tjernström, M., & Semedo, A. (2013). Global distribution and seasonal variability of coastal low-level jets derived from ERA-Interim reanalysis. *Tellus A: Dynamic Meteorology and Oceanography*, *65*(1), 20412. https://doi.org/10.3402/tellusa.v65i0.20412

Ranjha, R., Tjernström, M., Semedo, A., Svensson, G., & Cardoso, R. M. (2015). Structure and variability of the Oman coastal low-level jet. *Tellus A: Dynamic Meteorology and Oceanography*, *67*(1), 25285. https://doi.org/10.3402/tellusa.v67.25285

Ricciardulli, L., & Wentz, F. J. (2015). A scatterometer geophysical model function for climate-quality winds: QuikSCAT Ku-2011. *Journal of Atmospheric and Oceanic Technology*, *32*(10), 1829–1846. Retrieved from %3CGo

Ridgway, K. R., & Dunn, J. R. (2003). Mesoscale structure of the mean east Australian current system and its relationship with topography. *Progress in Oceanography*, *56*(2), 189–222. https://doi.org/10.1016/s0079-6611(03)00004-1

Rife, D. L., Pinto, J. O., Monaghan, A. J., Davis, C. A., & Hannan, J. R. (2010). Global distribution and characteristics of diurnally varying low-level jets. *Journal of Climate*, *23*(19), 5041–5064. https://doi.org/10.1175/2010JCLI3514.1

Rotunno, R. (1983). On the linear-theory of the land and sea Breeze. *Journal of the Atmospheric Sciences*, *40*(8), 1999–2009. https://doi.org/10.1175/1520-0469(1983)040<1999:OTLTOT>2.0.CO;2

Shapiro, A., Fedorovich, E., & Rahimi, S. (2016). A unified theory for the Great Plains nocturnal low-level jet. *Journal of the Atmospheric Sciences*, *73*(8), 3037–3057. https://doi.org/10.1175/jas-d-15-0307.1

Soares, P. M. M., Lima, D. C. A., Cardoso, R. M., & Semedo, A. (2017). High resolution projections for the western Iberian coastal low level jet in a changing climate. *Climate Dynamics*, *49*(5–6), 1547–1566. https://doi.org/10.1007/s00382-016-3397-8

Stensrud, D. J. (1996). Importance of low-level jets to climate: A review. *Journal of Climate*, *9*(8), 1698–1711. https://doi.org/10.1175/1520-0442(1996)009<1698:IOLLJT>2.0.CO;2

Winant, C. D., Dorman, C. E., Friehe, C. A., & Beardsley, R. C. (1988). The marine layer off northern California—An example of supercritical channel flow. *Journal of the Atmospheric Sciences*, *45*(23), 3588–3605. https://doi.org/10.1175/1520-0469(1988)045<3588:TMLONC>2.0.CO;2

Zhang, Q. H., Lau, K. H., Kuo, Y. H., & Chen, S. J. (2003). A numerical study of a mesoscale convective system over the Taiwan strait. *Monthly Weather Review*, *131*(6), 1150–1170. https://doi.org/10.1175/1520-0493(2003)131<1150:ANSOAM>2.0.CO;2